INTERNATIONAL CONGRESS FOR APPLIED MECHANICS JET'2018
2, 3 ET 4 MAI 2018, MARRAKECH - MAROC

Prédiction de la formabilité de bicouches métal/élastomère en utilisant des modèles de comportement élasto-plastique basés sur la plasticité cristalline

Formability prediction of metal/elastomer bilayers using elasto-plastic constitutive models based on crystal plasticity

Mohamed Ben Bettaieb, Farid Abed-Meraim

LEM3, UMR CNRS 7239 - Arts et Métiers ParisTech, 4 rue Augustin Fresnel, 57078 Metz Cedex 3, France

Email: Farid.Abed-Meraim@ensam.eu

Mots clés : Bicouches métal/élastomère, Courbes limites de formage, Striction localisée, Modèle Néo-Hookéen, Plasticité cristalline, Analyses de bifurcation et d'imperfection initiale

Keywords: Metal/elastomer bilayers, Forming limit diagrams, Localized necking, Neo-Hookean model, Rate-independent crystal plasticity, Bifurcation and imperfection analyses

RÉSUMÉ : Dans cette étude, la théorie de bifurcation et l'approche d'imperfection sont utilisées pour prédire la striction localisée dans des bicouches métal/élastomère. Le schéma auto-cohérent de transition d'échelles est adopté pour déduire le comportement polycristallin à partir de celui de ses constituants élémentaires (monocristaux). Le substrat d'élastomère, supposé en adhérence parfaite, suit un modèle hyper-élastique Néo-Hookéen. Les simulations montrent que les déformations limites prédites par l'approche d'imperfection tendent vers celles prédites par la théorie de bifurcation, lorsque la taille d'imperfection tend vers zéro. On montre également que l'ajout d'un substrat d'élastomère améliore la ductilité de la bicouche.

ABSTRACT: In this work, both the bifurcation theory and the imperfection approach are used to predict localized necking in metal/elastomer bilayers. The self-consistent scale-transition scheme is used to derive the behavior of the polycrystalline aggregate from that of its microscopic constituents (single crystals). As to the elastomer substrate, it follows a Neo-Hookean hyperelastic model. The adherence between the two layers is assumed to be perfect. The numerical results reveal that the limit strains predicted by the imperfection approach tend towards the bifurcation predictions when the size of the geometric imperfection vanishes. Also, it is shown that the addition of an elastomer layer to a metal layer enhances ductility.

I. INTRODUCTION

The ductility of a material is characterized by its ability to deform homogeneously under some imposed loading. For sheet metals undergoing in-plane biaxial loading, at a certain limit strain, the deformation starts concentrating in narrow bands. The occurrence of such localization bands marks the onset of localized necking in the sheet. Predicting the limit strains that lead to localized necking is crucial for designing functional or structural components used in industrial devices. To this end, several numerical models have been developed to predict localized necking, which is represented in the form of forming limit diagram (FLD). This FLD concept was initially introduced by Keeler and Backofen [1], for representing the limit strains in the range of positive strain paths, and has been extended by Goodwin [2] to the range of negative strain paths. Despite the wide range of FLD prediction models available in the literature, very few of them have been devoted to metal/elastomer bilayers. However, the latter have proven better stretchability than traditional freestanding metal layers, and are being increasingly used in the industry. For instance, in the design of electronic devices that require high levels of stretchability, substrate-supported metal layers are often used. This is the case of stretchable conductors used in biomedical applications, and interconnects that are used in large-scale integrated circuits [3,4]. The present paper proposes an efficient tool for the prediction of localized necking in substrate-supported metal layers. The mechanical behavior of a representative volume element of the metal layer is determined from the mechanical behavior of its microscopic constituents by using the self-consistent (SC) scale-transition scheme. Such a micromechanical approach allows an accurate description for the mechanical behavior of the metal layer. Indeed, the self-consistent model takes into account essential microstructure-related features that are relevant at the microscale. These microstructural aspects include key physical mechanisms, such as initial and induced crystallographic textures, morphological anisotropy, and interactions between grains and their surrounding medium. It is noteworthy that, in the literature, other alternatives to the self-consistent scheme are used as well. These alternatives are generally based on the finite element method (CPFEM), where spatial discretization by finite elements is generally required at both the polycrystalline aggregate and the single crystal scales. The mechanical behavior at the single crystal scale is described by a finite strain rate-independent constitutive framework, where the Schmid law is used to model the plastic flow. This rate-independent formulation is more suitable for the modeling and the simulation of cold forming processes, where viscous effects are limited. The developed model is applied in this paper to metal layers with FCC crystallographic structure. On the other hand, the mechanical behavior of the elastomer layer is assumed to obey a hyperelastic neo-Hookean constitutive law. The adherence between the two layers is assumed to be perfect. In order to predict localized necking in the bilayer, the overall mechanical behavior is coupled with two different localization criteria: the bifurcation theory, initially developed by Rice [5], and the imperfection approach initiated by Marciniak and Kuczynski [6]. The use of the Schmid law at the single crystal scale allows predicting limit strains at realistic levels when the bifurcation theory is used as localization criterion. One of the main conclusions of this paper is that the addition of an elastomer layer can significantly retard the occurrence of localized necking in the whole bilayer. It is also demonstrated that the FLDs of the bilayer predicted by the Marciniak–Kuczynski (M–K) analysis tend towards those predicted by the bifurcation theory in the limit of a vanishing size for the initial geometric imperfection of the metal layer.

The remainder of the paper is organized as follows: The constitutive equations describing the mechanical behavior of the metal and elastomer layers will be outlined in the second section. In the third section, the theoretical framework for the two localization criteria will be presented. Various numerical results obtained by the application of the developed tool will be presented and discussed in the fourth section.

II. MECHANICAL BEHAVIOR OF THE BILAYER

A. Metal Layer

1) Constitutive equations at the polycrystalline scale:

Let us consider a polycrystalline aggregate, which is assumed to be statistically representative of the metal layer. To derive the mechanical behavior of this polycrystalline aggregate from the behavior of its microscopic constituents, the self-consistent model is used. Only the main lines of this scheme are presented here; the complete details can be found in [7]. Compared to the full-constraint (FC) Taylor model, which is more commonly used due to its simplicity, the self-consistent scheme presents a number of advantages. Indeed, through the formulation of this scale-transition scheme, the equilibrium condition at the single crystal level is satisfied. Also, the grain morphology and the interactions between the grain and its surrounding medium are accounted for.

Because the behavior of the polycrystalline aggregate is modeled within the framework of finite strains, the nominal stress rate $\dot{\mathbf{N}}$ and the velocity gradient $\mathbf{G}$ are used as appropriate stress and strain measures, respectively. The macroscopic tangent modulus $\mathbf{L}$ linking $\dot{\mathbf{N}}$ to $\mathbf{G}$ is then obtained by using the self-consistent model

$$\dot{\mathbf{N}} = \mathbf{L} : \mathbf{G} . \tag{1}$$

The macroscopic velocity gradient $\mathbf{G}$ and nominal stress rate $\dot{\mathbf{N}}$ can be derived from their microscopic counterparts $\mathbf{g}$ and $\dot{\mathbf{n}}$ by using the averaging Hill theorem [8]

$$\mathbf{G} = \overline{\mathbf{g}(\mathbf{x})} \quad ; \quad \dot{\mathbf{N}} = \overline{\dot{\mathbf{n}}(\mathbf{x})} , \tag{2}$$

where $\mathbf{x}$ is a material point in the polycrystalline aggregate, and $\overline{\mathbf{a}}$ the average of field $\mathbf{a}$ over the volume V of the polycrystalline aggregate. Conversely, the microscopic velocity gradient and nominal stress rate are linked to their macroscopic counterparts by the following relations:

$$\mathbf{g}(\mathbf{x}) = \mathbf{A}(\mathbf{x}) : \mathbf{G} \quad ; \quad \dot{\mathbf{n}}(\mathbf{x}) = \mathbf{B}(\mathbf{x}) : \dot{\mathbf{N}}, \tag{3}$$

where $\mathbf{A}(\mathbf{x})$ and $\mathbf{B}(\mathbf{x})$ are fourth-order concentration tensors for the velocity gradient and nominal stress rate, respectively.

At the microscale, a behavior law similar to (1) can be found by combining the single crystal constitutive relations

$$\dot{\mathbf{n}}(\mathbf{x}) = \mathbf{l}(\mathbf{x}) : \mathbf{g}(\mathbf{x}), \tag{4}$$

where $\mathbf{l}$ is the microscopic tangent modulus. Also, it is assumed that all mechanical variables are homogeneous within the individual single crystals. Thus, for any single crystal I within the polycrystalline aggregate (I =1, …, N_g), one has:

$$\dot{\mathbf{n}}^I = \mathbf{l}^I : \mathbf{g}^I, \tag{5}$$

with N_g the number of grains in the polycrystalline aggregate.

A preliminary straightforward relation between $\mathbf{L}$ and $\mathbf{l}$ can be easily obtained by combining the above equations

$$\mathbf{L} = \overline{\mathbf{l}(\mathbf{x}) : \mathbf{A}(\mathbf{x})}. \tag{6}$$

By using Green's tensor, the concentration tensor $\mathbf{A}^I$ is obtained after some elaborate mathematical developments

$$\mathbf{A}^I = (\mathbf{I} - \mathbf{T}^{II} : (\mathbf{l}^I - \mathbf{L}))^{-1} : \overline{(\mathbf{I} - \mathbf{T}^{II} : (\mathbf{l}^I - \mathbf{L}))^{-1}}^{-1}, \tag{7}$$

where $\mathbf{T}^{II}$ is a fourth-order tensor, which is function of $\mathbf{L}$, that describes the interaction between grain I and its surrounding medium. The macroscopic tangent modulus derived by the 1-site self-consistent version of the incremental scheme of Hill [8] can be finally obtained as follows:

$$\mathbf{L} = \sum_{I=1}^{N_g} f^I \mathbf{l}^I : \mathbf{A}^I, \tag{8}$$

where f^I is the volume fraction of single crystal I.

Equations (7)-(8) represent a non-linear system, which is incrementally solved by using the iterative fixed point method. Note that the full-constraint Taylor model can be easily deduced from the self-consistent approach, by reducing all concentration tensors $\mathbf{A}^I$ to the fourth-order identity tensor.

2) Constitutive equations at the single crystal scale:

The microscopic velocity gradient is additively split into its symmetric and skew-symmetric parts, denoted $\mathbf{d}$ and $\mathbf{w}$

$$\mathbf{d} = (1/2)(\mathbf{g} + \mathbf{g}^{\mathrm{T}}) \quad ; \quad \mathbf{w} = (1/2)(\mathbf{g} - \mathbf{g}^{\mathrm{T}}). \tag{9}$$

Additionally, the strain tensor $\mathbf{d}$ and the spin tensor $\mathbf{w}$ are split into their elastic and plastic parts

$$\mathbf{d} = \mathbf{d}^{\mathrm{e}} + \mathbf{d}^{\mathrm{p}} \quad ; \quad \mathbf{w} = \mathbf{w}^{\mathrm{e}} + \mathbf{w}^{\mathrm{p}}. \tag{10}$$

The rotation $\mathbf{r}$ of the single crystal lattice frame is related to the elastic part of the spin tensor $\mathbf{w}^{\mathrm{e}}$ as follows:

$$\dot{\mathbf{r}}.\mathbf{r}^{\mathrm{T}} = \mathbf{w}^{\mathrm{e}}. \tag{11}$$

To satisfy the objectivity principle, the co-rotational rate $\boldsymbol{\sigma}^{\nabla}$ of the Cauchy stress tensor, with respect to the lattice rotation, is related to the elastic strain rate $\mathbf{d}^{\mathrm{e}}$ as follows:

$$\boldsymbol{\sigma}^{\nabla} = \dot{\boldsymbol{\sigma}} - \mathbf{w}^{\mathrm{e}}.\boldsymbol{\sigma} + \boldsymbol{\sigma}.\mathbf{w}^{\mathrm{e}} = \mathbf{C}^{\mathrm{e}} : \mathbf{d}^{\mathrm{e}}, \tag{12}$$

where $\mathbf{C}^{\mathrm{e}}$ is the fourth-order elasticity tensor.

The inelastic deformation being only due to the slip on the crystallographic planes, $\mathbf{d}^{\mathrm{p}}$ and $\mathbf{w}^{\mathrm{p}}$ are given as follows:

$$\mathbf{d}^{\mathrm{p}} = \sum_{\beta=1}^{N_s} \dot{\gamma}^\beta \operatorname{sgn}(\tau^\beta)\mathbf{R}^\beta \; ; \; \mathbf{w}^{\mathrm{p}} = \sum_{\beta=1}^{N_s} \dot{\gamma}^\beta \operatorname{sgn}(\tau^\beta)\mathbf{S}^\beta, \tag{13}$$

with N_s the total number of slip systems, $\dot{\gamma}^\beta$ the slip rate of slip system β, $\mathbf{R}^\beta$ (resp. $\mathbf{S}^\beta$) the symmetric (resp. skew-symmetric) part of the Schmid orientation tensor, and τ^β the resolved shear stress of slip system β, equal to $\boldsymbol{\sigma} : \mathbf{R}^\beta$.

Within an updated Lagrangian framework, the nominal stress rate $\dot{\mathbf{n}}$ can be expressed by the following relation:

$$\dot{\mathbf{n}} = \dot{\boldsymbol{\sigma}} + \boldsymbol{\sigma}\operatorname{Tr}(\mathbf{d}) - \mathbf{g}.\boldsymbol{\sigma}, \tag{14}$$

which, combined with the above equations, gives

$$\begin{aligned} \dot{\mathbf{n}} = {} & (\mathbf{C}^{\mathrm{e}} + \boldsymbol{\sigma} \otimes \mathbf{I}_2) : \mathbf{d} - \boldsymbol{\sigma}.\mathbf{w} - \mathbf{d}.\boldsymbol{\sigma} \\ & - \sum_{\beta \in \mathcal{A}} \operatorname{sgn}(\tau^\beta)\left(\mathbf{C}^{\mathrm{e}} : \mathbf{R}^\beta + \mathbf{S}^\beta.\boldsymbol{\sigma} - \boldsymbol{\sigma}.\mathbf{S}^\beta\right)\dot{\gamma}^\beta, \end{aligned} \tag{15}$$

where $\mathcal{A}$ denotes the set of active slip systems. The consistency condition associated with the active slip systems, which derives from the Schmid law, can be expressed as

$$\forall \beta \in \mathcal{A} : \; \dot{\chi}^\beta = \operatorname{sgn}(\tau^\beta)\dot{\tau}^\beta - \dot{\tau}_{\mathrm{c}}^\beta = 0 \quad ; \quad \dot{\gamma}^\beta > 0, \tag{16}$$

where τ_{c}^β is the critical shear stress of slip system β, whose evolution is described by the following hardening law:

$$\begin{aligned} & \forall \beta \in \mathcal{A} : \quad \dot{\tau}_{\mathrm{c}}^\beta = h \sum_{\alpha \in \mathcal{A}} \dot{\gamma}^\alpha \\ & h = h_0 \left(1 + \frac{h_0 \, \Gamma}{\tau_0 \, n}\right)^{n-1} \quad ; \quad \Gamma = \sum_{\alpha=1}^{N_s} \gamma^\alpha, \end{aligned} \tag{17}$$

where h_0 is the initial hardening rate, n the power-law hardening exponent, and τ_0 the initial critical shear stress.

The slip rates of the active slip systems are finally obtained by combining (12, 13_1, 17) with the consistency condition (16)

$$\dot{\gamma}^\beta = \sum_{\alpha\in\mathcal{A}} M^{\beta\alpha}\,\mathrm{sgn}(\tau^\alpha)\,\mathbf{R}^\alpha : \mathbf{C}^{\mathrm{e}} : \mathbf{d} = \mathbf{y}^\beta : \mathbf{d}\,, \qquad (18)$$

where $\mathbf{M}$ is the inverse of matrix $\mathbf{P}$, defined as follows:

$$\forall \alpha,\beta \in \mathcal{A}:\ P^{\alpha\beta} = \left(h + \mathrm{sgn}(\tau^\alpha)\,\mathrm{sgn}(\tau^\beta)\,\mathbf{R}^\alpha : \mathbf{C}^{\mathrm{e}} : \mathbf{R}^\beta\right) \qquad (19)$$

Combining (4), (15) and (18), one can obtain the analytical expression of the microscopic tangent modulus $\mathbf{l}$

$$\begin{aligned}\mathbf{l} = {} & \mathbf{C}^{\mathrm{e}} + \boldsymbol{\sigma}\otimes\mathbf{I}_2 - {}^1\boldsymbol{\Lambda}(\boldsymbol{\sigma}) - {}^2\boldsymbol{\Lambda}(\boldsymbol{\sigma}) \\ & - \sum_{\alpha\in\mathcal{A}} \mathrm{sgn}(\tau^\alpha)\left(\mathbf{C}^{\mathrm{e}} : \mathbf{R}^\alpha + \mathbf{S}^\alpha.\boldsymbol{\sigma} - \boldsymbol{\sigma}.\mathbf{S}^\alpha\right)\otimes\mathbf{y}^\alpha\end{aligned} \qquad (20)$$

where ${}^1\boldsymbol{\Lambda}$ and ${}^2\boldsymbol{\Lambda}$ are fourth-order tensors that reflect the contribution of Cauchy stress convective terms

$${}^1\Lambda_{ijkl}(\boldsymbol{\sigma}) = \frac{1}{2}(\delta_{lj}\sigma_{ik} - \delta_{kj}\sigma_{il})\ ;\ {}^2\Lambda_{ijkl}(\boldsymbol{\sigma}) = \frac{1}{2}(\delta_{ik}\sigma_{lj} + \delta_{il}\sigma_{kj}) \qquad (21)$$

The above highly nonlinear constitutive equations are integrated incrementally over each time increment, using an implicit ultimate algorithm similar to that developed in [9].

B. Elastomer Layer

The behavior of the elastomer layer is modeled by a hyperelastic neo-Hookean law [10]. This model relates the Cauchy stress tensor $\boldsymbol{\Sigma}$ to the left Cauchy-Green tensor $\mathbf{V}$

$$\boldsymbol{\Sigma} = q\,\mathbf{I}_2 + \mu\,\mathbf{V}^2\,, \qquad (22)$$

where μ is the shear modulus, q is an unknown hydrostatic pressure to be determined by applying the incompressibility constraint, and $\mathbf{V}$ is defined by the following relation:

$$\mathbf{V}^2 = \mathbf{F}.\mathbf{F}^{\mathrm{T}}\,, \qquad (23)$$

with $\mathbf{F}$ the deformation gradient tensor of the elastomer layer.

III. Strain Localization Criteria

Let us consider a bilayer consisting of a metal layer M and an elastomer layer E. These layers are assumed to be perfectly adhered and sufficiently thin. The small thickness assumption allows formulating the two above-mentioned localization criteria, namely the bifurcation theory and the initial imperfection approach, under the plane-stress conditions.

A. Bifurcation Theory

The bilayer is submitted to uniform strain, where the in-plane strain rates are equal to $\dot{E}_{11} = 1$, $\dot{E}_{22} = \rho$ and $\dot{E}_{12} = 0$. ρ is the strain-path ratio ranging from −1/2 (uniaxial tensile state) to 1 (equibiaxial tensile state). Considering the plane-stress conditions, this specific loading implies that the macroscopic velocity gradient and the macroscopic nominal stress rate tensor have the following generic forms:

$$\mathbf{G} = \begin{pmatrix} 1 & 0 & 0 \\ 0 & \rho & 0 \\ 0 & 0 & ? \end{pmatrix} \quad ; \quad \dot{\mathbf{N}} = \begin{pmatrix} ? & ? & 0 \\ ? & ? & 0 \\ 0 & 0 & 0 \end{pmatrix}, \qquad (24)$$

where symbol ? designates the unknown components in both tensors. These generic forms are valid for both layers.

The bifurcation criterion states that strain localization occurs when the acoustic tensor becomes singular. Hence, this criterion is expressed in the following mathematical form:

$$\det\left(\vec{\mathcal{N}}^{\mathrm{PS}}.\mathbf{L}^{\mathrm{PS}}.\vec{\mathcal{N}}^{\mathrm{PS}}\right) = 0\,, \qquad (25)$$

where $\vec{\mathcal{N}}^{\mathrm{PS}}$ is the unit vector normal to the localization band. As to $\mathbf{L}^{\mathrm{PS}}$, it represents the averaged plane-stress tangent modulus of the bilayer, which is given by

$$\mathbf{L}^{\mathrm{PS}} = \frac{h_{\mathrm{M}}\,\mathbf{L}^{\mathrm{PS}}_{\mathrm{M}} + h_{\mathrm{E}}\,\mathbf{L}^{\mathrm{PS}}_{\mathrm{E}}}{h_{\mathrm{M}} + h_{\mathrm{E}}}\,, \qquad (26)$$

where h_{M} (resp. h_{E}) is the initial thickness of the metal (resp. elastomer) layer, and $\mathbf{L}^{\mathrm{PS}}_{\mathrm{M}}$ (resp. $\mathbf{L}^{\mathrm{PS}}_{\mathrm{E}}$) is the plane-stress tangent modulus of the metal (resp. elastomer) layer. Note that $\mathbf{L}^{\mathrm{PS}}_{\mathrm{M}}$ is derived from the 3D expression of the metal layer tangent modulus $\mathbf{L}_{\mathrm{M}}$ by the following condensation relation:

$$\forall \alpha,\beta,\gamma,\delta = 1,2:\quad L^{\mathrm{PS}}_{\mathrm{M}\,\alpha\beta\gamma\delta} = L_{\mathrm{M}\,\alpha\beta\gamma\delta} - \frac{L_{\mathrm{M}\,\alpha\beta 33}\ L_{\mathrm{M}\,33\gamma\delta}}{L_{\mathrm{M}\,3333}}. \qquad (27)$$

As to tensor $\mathbf{L}^{\mathrm{PS}}_{\mathrm{E}}$, it is given by the following relation [11]:

$$\mathbf{L}^{\mathrm{PS}}_{\mathrm{E}} = \boldsymbol{\mathcal{L}} + \boldsymbol{\Sigma}\otimes\mathbf{I}_2 - {}^1\boldsymbol{\Lambda}(\boldsymbol{\Sigma}) - {}^2\boldsymbol{\Lambda}(\boldsymbol{\Sigma})\,, \qquad (28)$$

in which the non-zero components of tensor $\boldsymbol{\mathcal{L}}$ are defined by

$$\begin{cases} \mathcal{L}_{1111} = 2\,\mu[\mathrm{e}^{2E_{11}} + \mathrm{e}^{-2(E_{11}+E_{22})}] \\ \mathcal{L}_{2222} = 2\,\mu[\mathrm{e}^{2E_{22}} + \mathrm{e}^{-2(E_{11}+E_{22})}] \\ \mathcal{L}_{1122} = 2\,\mu\,\mathrm{e}^{-2(E_{11}+E_{22})} \\ \mathcal{L}_{1212} = \dfrac{\mu}{2}[\mathrm{e}^{2E_{11}} + \mathrm{e}^{2E_{22}}]. \end{cases} \qquad (29)$$

For each strain-path ratio ρ, and at each time increment, the bifurcation criterion (25) is checked for all possible band orientations ($\theta \in [0, \pi/2]$). When the acoustic tensor becomes

singular for a given band orientation, the computation is stopped. The overall major strain E_{11}, thus determined, represents the localization limit strain, while the associated angle θ corresponds to the necking band orientation.

B. Initial Imperfection Approach

For the application of the imperfection approach (denoted M–K analysis) to the bilayer, we assume the preexistence of a groove in the form of a band in the metal layer (see Fig. 1).

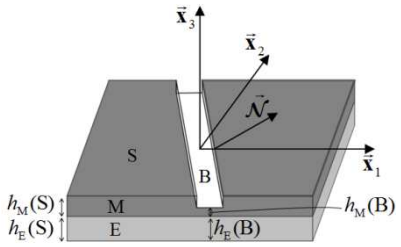

Fig. 1. M–K analysis for a bilayer (initial geometry and band orientation).

The initial imperfection ratio ξ_0 can be defined as (Fig. 1)

$$\xi_0 = 1 - \frac{h_M(B)}{h_M(S)}. \tag{30}$$

The M–K analysis is based on four main sets of equations:

- As a consequence of the perfect adherence between the metal and elastomer layers, the following equalities between the in-plane velocity gradients in the metal layer and their counterparts in the elastomer layer hold:

$$\begin{aligned} \mathbf{G}_M^{PS}(B) &= \mathbf{G}_E^{PS}(B) = \mathbf{G}^{PS}(B) \\ \mathbf{G}_M^{PS}(S) &= \mathbf{G}_E^{PS}(S) = \mathbf{G}^{PS}(S). \end{aligned} \tag{31}$$

- The kinematic compatibility condition between the band and the safe zone (i.e., outside the band) must be satisfied, which requires that the displacement increments be continuous across the band, namely:

$$\mathbf{G}^{PS}(B) = \mathbf{G}^{PS}(S) + \dot{\vec{\mathbf{C}}}^{PS} \otimes \vec{\mathcal{N}}^{PS}. \tag{32}$$

- The equilibrium balance across the interface between the band and the safe zone, which writes

$$\begin{aligned} &\vec{\mathcal{N}}^{PS}.(h_M(B)\,\dot{\mathbf{N}}_M^{PS}(B) + h_E(B)\,\dot{\mathbf{N}}_E^{PS}(B)) \\ &= \vec{\mathcal{N}}^{PS}.(h_M(S)\,\dot{\mathbf{N}}_M^{PS}(S) + h_E(S)\,\dot{\mathbf{N}}_E^{PS}(S)). \end{aligned} \tag{33}$$

- The constitutive equations both for the metal layer and the elastomer layer, restricted to the plane dimension inside and outside the band, respectively, which can be expressed in the following generic form:

$$\begin{aligned} &\dot{\mathbf{N}}_M^{PS}(B) = \mathbf{L}_M^{PS}(B) : \mathbf{G}^{PS}(B) \;\; ; \;\; \dot{\mathbf{N}}_E^{PS}(B) = \mathbf{L}_E^{PS}(B) : \mathbf{G}^{PS}(B) \\ &\dot{\mathbf{N}}_M^{PS}(S) = \mathbf{L}_M^{PS}(S) : \mathbf{G}^{PS}(S) \;\; ; \;\; \dot{\mathbf{N}}_E^{PS}(S) = \mathbf{L}_E^{PS}(S) : \mathbf{G}^{PS}(S). \end{aligned} \tag{34}$$

For each strain-path ratio ρ and each initial band orientation θ_0, the above equations that govern the M–K approach are integrated incrementally over each time increment. The computations are stopped when the norm of the jump vector $\dot{\vec{\mathbf{C}}}^{PS}$ increases rapidly, thus marking the localization of the deformation in the band zone. Further numerical and algorithmic details regarding the M–K approach can be found in [11].

IV. Prediction Results

A. Material and Geometric Data

The polycrystalline aggregate studied in this paper is made of 2000 grains. Its initial crystallographic texture is generated randomly (see Fig. 2) in such a way that it is orthotropic with respect to the rolling and transverse directions. Note that it is well known that the initial crystallographic texture strongly affects both the shape and the overall level of the predicted FLDs. Here, initially, all of the grains are assumed to be spherical with the same volume fraction. Also, we assume that the adopted polycrystalline aggregate is representative of the studied metal sheet. Several literature studies have suggested that at least 1000 grains are required for the polycrystalline aggregate to be representative of the studied material. From a number of numerical simulations (that have been conducted, but not included in this paper for conciseness), it is observed that beyond 2000 grains, the response of the polycrystalline aggregate representing the metal layer remains almost unchanged. As plastic strain localization occurs at relatively large strains, the values of limit strains are almost unaffected by the elastic behavior. This justifies the consideration of simple isotropic elastic behavior in the current study.

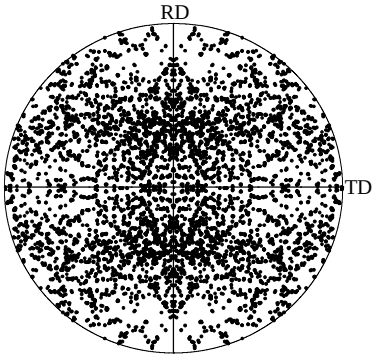

Fig. 2. Initial crystallographic texture of the studied polycrystalline aggregate: {111} pole figure.

The material parameters of the single crystals are given in Table 1. The elastic parameters are representative of steel materials. As to hardening parameters, they are the same as those used in [12].

TABLE I. MATERIAL PARAMETERS FOR THE SINGLE CRYSTALS

Elasticity		Hardening		
E [GPa]	ν	τ_0 [MPa]	h_0 [MPa]	n
210	0.3	40	390	0.35

The shear modulus of the elastomer layer is set to 22 MPa. This choice is based on data for polyurea [13]. The ratio between the initial thickness of the elastomer layer and the initial thickness of the metal layer is taken equal to 0.5.

B. Bifurcation Theory Predictions

The evolution of the minimum of the cubic root of the determinant of the acoustic tensor, over all possible band orientations, as a function of the major strain E_{11} is displayed in Fig. 3. The onset of strain localization is detected when this minimum reaches 0, as defined by the bifurcation criterion (25). The self-consistent approach is used as scale-transition scheme. Four representative strain paths are considered in this figure: ρ =–0.5, ρ =0, ρ =0.5, and ρ =1. By comparing Fig. 3 (left) and Fig. 3 (right), one can observe that the presence of the elastomer layer substantially retards the occurrence of strain localization. This result is the consequence of the fact that under biaxial loading, the tangent modulus of the elastomer remains unchanged, or increases, while the tangent modulus of the metal layer steadily decreases.

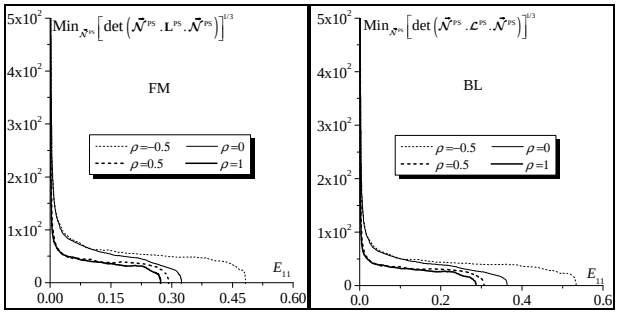

Fig. 3. Evolution of the minimum of the cubic root of the determinant of the acoustic tensor, as a function of the major strain E_{11}, for four representative strain paths (ρ =–0.5, ρ =0, ρ =0.5, and ρ =1): (left) Freestanding metal layer; (right) Metal/elastomer bilayer.

The effect of the elastomer layer on necking retardation for all strain paths $\rho \in [-1/2, 1]$ is investigated in Fig. 4. This figure confirms the preliminary result obtained in Fig. 3: the elastomer layer allows shifting the FLD monotonically upwards, and thus enhances the ductility of the bilayer.

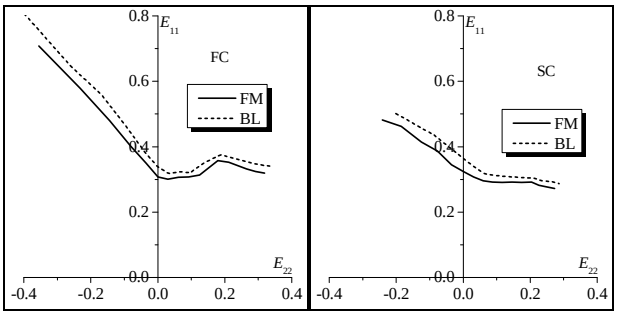

Fig. 4. Effect of the elastomer layer on the improvement of the formability of the bilayer (represented in terms of FLD): (left) FC model; (right) SC model.

C. M–K Analysis Predictions

In order to illustrate the onset of strain localization, the evolution of the in-plane components of the jump vector $\dot{\vec{\mathbf{C}}}$ and the determinant of the acoustic tensor in the band are plotted in Fig. 5 as function of the major strain in the safe zone E_{11}. In this simulation, the strain-path ratio ρ, the initial imperfection ratio ξ_0 and the initial band orientation θ_0 are set to 0, 10^{-3} and 0°, respectively. The SC model is used for the transition between the microscopic and macroscopic scales in the metal layer. It is clear from Fig. 5 (left) that the jump vector $\dot{\vec{\mathbf{C}}}$ remains very close to $\vec{\mathbf{0}}$ before strain localization. This jump vector, and especially its first component, increases very abruptly when the strain in the safe zone E_{11} is about 0.28, thus leading to the localization of deformation within the band. The evolution of the determinant of the acoustic tensor in the band is reported in Fig. 5 (right). The limit strain (0.28) is reached when this determinant becomes equal to 0. This result is expectable considering the similarity in the mathematical formulation of the bifurcation theory and the M–K approach. The evolution of this determinant can be used as a reliable alternative indicator of strain localization for the different strain paths.

The comparison between the FLDs predicted by bifurcation theory and those determined by M–K analysis is shown in Fig. 6. Three different values for the initial imperfection ratio ξ_0 are considered: 10^{-4}, 10^{-3} and 10^{-2}. It is clear that the shape and the level of the predicted FLDs are significantly influenced by the amount of initial geometric imperfection. It is also found that for all strain paths, the limit strains predicted by bifurcation theory set an upper bound to those yielded by the M–K approach. Moreover, this result is valid for both scale-transition schemes, namely the full-constraint (FC) and self-consistent (SC) models.

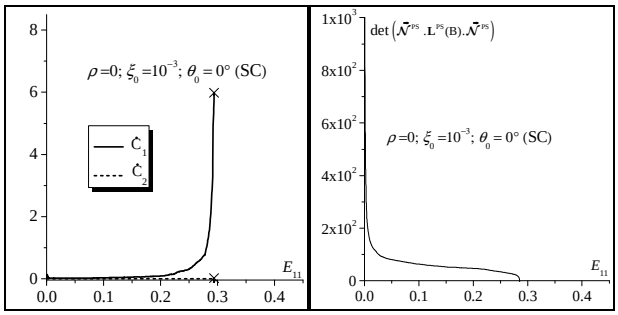

Fig. 5. Illustration of the onset of strain localization (bilayer; ρ=0; ξ_0=10^{-3}; θ_0=0°; SC): (left) Evolution of the in-plane components of the jump vector $\dot{\mathbf{C}}$ as a function of the major strain in the safe zone E_{11}; (right) Evolution of the determinant of the acoustic tensor in the band as a function of the major strain in the safe zone E_{11}.

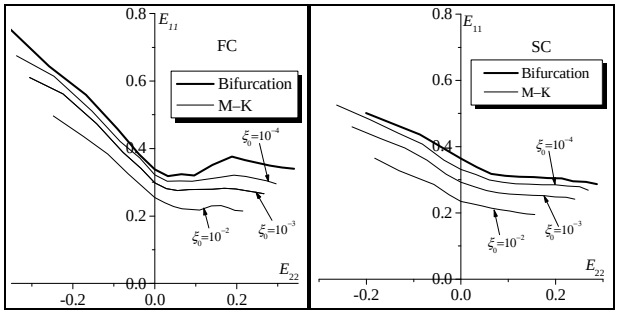

Fig. 6. Effect of the initial geometric imperfection on the shape and the level of the FLDs of the bilayer: (left) FC model; (right) SC model.

V. Concluding Remarks

In this work, a powerful tool has been developed to predict the onset of localized necking in metal/elastomer bilayers. In this tool, the behavior of the metal (resp. elastomer) layer is modeled by the self-consistent micromechanical model (resp. neo-Hookean hyperelastic model). The constitutive modeling of the bilayer is coupled with two strain localization criteria to predict the limit strains: the bifurcation theory and the imperfection approach. From the predictions obtained by applying this tool, three main conclusions can be drawn:

- The presence of an elastomer layer increases substantially the level of limit strains for the bilayer.
- The shape and the level of the predicted FLDs are significantly affected by the size of initial imperfection.
- The limit strains predicted by the bifurcation theory set an upper bound to those yielded by the M–K approach.

References

[1] S.P. Keeler and W.A. Backofen, "Plastic instability and fracture in sheets stretched over rigid punches," Trans. ASM, vol. 56, pp. 25-48, 1963.

[2] G.M. Goodwin, "Application of strain analysis to sheet metal forming problems in the press shop," Metallurgia Italiana, vol. 60, pp. 767-774, 1968.

[3] S.L. Chiu, J. Leu, and P.S. Ho, "Fracture of metal-polymer line structures. I. Semiflexible polyimide," J. Appl. Phys., vol. 76, pp. 5136-5142, 1994.

[4] M. Hommel and O. Kraft, "Deformation behavior of thin copper films on deformable substrates," Acta Mater., vol. 49, pp. 3935-3947, 2001.

[5] J.R. Rice, "The localization of plastic deformation," in Proc. of 14th International Congress of Theoretical and Applied Mechanics, vol. 1, W.T. Koiter, Ed. North-Holland Publishing Co., 1976, pp. 207-220.

[6] Z. Marciniak and K. Kuczynski, "Limit strains in the processes of stretch-forming sheet metal," Int. J. Mech. Sci., vol. 9, pp. 609-620, 1967.

[7] P. Lipinski, M. Berveiller, E. Reubrez, and J. Morreale, "Transition theories of elastic-plastic deformation of metallic polycrystals," Arch. Appl. Mech., vol. 65, pp. 291-311, 1995.

[8] R. Hill, "On constitutive macro-variables for heterogeneous solids at finite strain," Proc. Roy. Soc. London, vol. 326, pp. 131-147, 1972.

[9] H.K. Akpama, M. Ben Bettaieb, and F. Abed-Meraim, "Numerical integration of rate-independent BCC single crystal plasticity models: comparative study of two classes of numerical algorithms," Int. J. Num. Meth. Eng., vol. 108, pp. 363-422, 2016.

[10] S.C. Hunter, "Some exact solutions in the theory of finite elasticity for incompressible neo-Hookean materials," Int. J. Mech. Sci., vol. 21, pp. 203-211, 1979.

[11] M. Ben Bettaieb and F. Abed-Meraim, "Investigation of localized necking in substrate-supported metal layers: Comparison of bifurcation and imperfection analyses," Int. J. Plast., vol. 65, pp. 168-190, 2015.

[12] K. Yoshida and M. Kuroda, "Comparison of bifurcation and imperfection analyses of localized necking in rate-independent polycrystalline sheets," Int. J. Solids Struct., vol. 49, pp. 2073-2084, 2012.

[13] A.V. Amirkhizi, J. Isaacs, J. McGee, and S. Nemat-Nasser, "An experimentally-based viscoelastic constitutive model for polyurea, including pressure and temperature effects," Philos. Mag., vol. 86, pp. 5847-5866, 2006.